

LETTER TO THE EDITOR

# IRAM 04191+1522: a compact proto-brown dwarf binary candidate <sup>★</sup>

N. Huélamo<sup>1</sup>, I. de Gregorio-Monsalvo<sup>2</sup>, Aina Palau<sup>3</sup>, C. Carrasco-González<sup>3</sup>, A. Ribas<sup>4</sup>, H. Bouy<sup>5</sup>, R. Pandey<sup>3</sup>, D. Barrado<sup>1</sup>, N. Otten<sup>6</sup>, V.D. Ivanov<sup>7</sup>, M.F. Sterzik<sup>7</sup>, M. Dunham<sup>8</sup>, L. A. Zapata<sup>3</sup>, E. Pantin<sup>9</sup>, and E. Macias<sup>7</sup>

<sup>1</sup> Centro de Astrobiología (CAB), CSIC-INTA, ESAC Campus, Camino bajo del Castillo s/n, E-28692 Villanueva de la Cañada, Madrid, Spain

e-mail: nhuelamo@cab.inta-csic.es

<sup>2</sup> European Southern Observatory, Alonso de Cordova 3107, Casilla 19, Vitacura, Santiago, Chile

<sup>3</sup> Instituto de Radioastronomía y Astrofísica, Universidad Nacional Autónoma de México, Antigua Carretera a Pátzcuaro 8701, Ex-Hda. San José de la Huerta, 58089 Morelia, Michoacán, México

<sup>4</sup> Institute of Astronomy, University of Cambridge, Madingley Road, CB3 0HA Cambridge, UK

<sup>5</sup> Laboratoire d'Astrophysique de Bordeaux, Univ. Bordeaux, CNRS, B18N, allée Geoffroy Saint-Hilaire, 33615 Pessac, France

<sup>6</sup> Department of Physics, Maynooth University, Maynooth, Co.Kildare, Ireland

<sup>7</sup> European Southern Observatory, Karl-Schwarzschild-Strasse 2, 85748 Garching bei München, Germany

<sup>8</sup> Department of Physics, Middlebury College, Middlebury, VT 05753, USA

<sup>9</sup> Université Paris-Saclay, Université Paris Cité, CEA, CNRS, AIM, 91191, Gif-sur-Yvette, France

Received ; accepted

## ABSTRACT

**Context.** Very low-luminosity objects in nearby star-forming regions have been identified as promising proto-brown dwarf candidates. The study of their multiplicity can shed light on the dominant formation mechanism of these substellar objects.

**Aims.** We aim at studying the multiplicity of the very low luminosity object Iram 04191+1522.

**Methods.** We have obtained 0.89 mm ALMA observations with a very extended configuration, achieving an angular resolution of  $\sim 0''.04$  (6 au at 140 pc). We have complemented our data with new VLA observations, and ALMA archival data at 1.3 mm.

**Results.** We resolve Iram 04191+1522 into a close binary candidate for the first time. The binary is detected in the ALMA continuum data with a projected separation of  $\sim 80$  mas, or 11 au at a distance of 140 pc. The two sources are oriented in the East-West direction, with the eastern component being brighter and more extended than the western one, which is marginally resolved. The analysis of C<sup>18</sup>O(2-1) archival data reveals gaseous material in rotation around the binary, presumably from a circumbinary disk with  $\sim 27$  au of radius centered on the faintest ALMA component. A fit of the position-velocity diagram allows us to estimate a total dynamical mass for the system of  $50 \pm 40 M_{\text{Jup}}$ . Therefore, we classify Iram 04191 as a tight proto-brown dwarf binary candidate. The VLA data reveals the detection of a single object closer to the western ALMA source, and with a spectral index consistent with a radio jet.

**Key words.** Brown Dwarf Formation – binaries – individual: Iram 04191+1522

## 1. Introduction

Very low luminosity objects (VeLLOs), discovered by the *Spitzer* space telescope, are defined as embedded objects with internal luminosities ( $L_{\text{int}}$ ) below  $0.1 L_{\odot}$  (di Francesco et al. 2007). They have been identified as promising proto-brown dwarf (proto-BD) candidates, that is, BDs at the earliest stages of their evolution when they are still embedded in their parental clouds (see review by Palau et al. 2024). The multiplicity of proto-BDs is an important output of substellar formation theories, and its study can help to shed light on their dominant formation mechanism (e.g. Bate 2012; Offner et al. 2016).

We designed a pilot project to study the multiplicity of VeLLOs with ALMA, obtaining observations for Iram 04191+1522 (Iram 04191, hereafter). Iram 04191 is a Class 0 object located in the southern part of the Taurus molecular cloud, displaying a collimated CO(2-1) bipolar outflow and an ionized jet (André et al. 1999). It was detected by the *Spitzer* telescope at wavelengths shorter than  $60 \mu\text{m}$ , and classified as a VeLLO based on its  $L_{\text{int}}$  of  $0.08 \pm 0.04 L_{\odot}$  (Dunham et al.

2006). In this letter, we present unprecedented angular resolution ALMA observations of Iram 04191 at 0.89 mm that have allowed us to resolve the object into a tight binary candidate. We have complemented these data with new Very Large Array (VLA) observations, and ALMA Band 6 (1.3 mm) archival data.

## 2. Observations and data reduction

### 2.1. Band 7 ALMA observations

Iram 04191 was observed with the ALMA 12m-array on 24 November 2017, as part of the ALMA Cycle 5 program 2017.1.00551.S (PI Huélamo). The data were obtained with 49 antennas in single field dual polarization mode. Band 7 (334.9 GHz, 0.89 mm) was used, with two basebands centered at 335.9 and 334.0 GHz, respectively, both with a width of 1.875 GHz and a channel spacing of 31 MHz. We also placed two spectral windows centered at a frequency that contains the CO(3-2) and H<sup>13</sup>CO+(4-3) transitions, respectively, to obtain serendipitous detections of gas emission associated to outflow and disk phenomena. The observations were performed with an average precipitable water-vapor column of  $\sim 0.6$  mm. The antenna base-

<sup>★</sup> Based on observations obtained at the ALMA Observatory under programs 2017.1.00551.S and 2016.1.00039.S.

lines ranged from 92 m to 8.5 km, providing a maximum recoverable scale of  $0''.6$ . QSO J0237+2848 and QSO J0440+1437 were used as bandpass and phase calibrator, respectively. The former was used to scale the flux density. The science time on-source was 16 minutes. We used the automatic self-calibration pipeline `auto_selfcal`<sup>1</sup> to self-calibrate the visibilities and perform continuum imaging (Tobin et al. 2025), changing the `minsnr_to_proceed` parameter to be 1.5 instead of 2.95. The pipeline was executed using the Common Astronomy Software Applications package (CASA, McMullin et al. 2007) version 6.6.4. The data self-calibrated successfully, with the phase-only self-calibration converging down to the scan-length solution interval. We analyzed data with different imaging options (see Appendix B), selecting the image with robust  $-0.25$  and a cut in  $uv$ -range of  $> 200 k\lambda$  as our fiducial image (synthesized beam size of  $33\times 25$  mas, and PA of  $42^\circ$ ).

## 2.2. VLA observations

We observed IRAM04191 with the VLA of the National Radio Astronomy Observatory (NRAO) in its A configuration at K, Ka and Q bands (project 24B-250). All observations were performed during the second semester of 2024; October 22 for Q band, and December 4 and 5 for Ka and K, respectively. At all bands, we used the standard continuum observing setup which allows us to use a total of 8 GHz bandwidth for each band. For all bands, 3C147 was used as flux calibrator, 3C84 as the bandpass calibrator, and J0409+1217 as complex gain calibrator. At each band, we used cycles between target and complex gain calibrator as recommended for A configuration by the NRAO. Data were calibrated by the NRAO staff using CASA v6.6.1 and the VLA pipeline. We tried self-calibration of the data, but it did not work due to the faintness of the source. Images were made using `tclean` from the calibrated data and exploring different visibility weightings (natural, uniform and briggs). We have produced a single image combining all three bands (KKaQ) and using multi-frequency synthesis. We have worked with the image with a robust parameter of 1, showing a synthesized beam size of  $0''.08\times 0''.07$ , and PA of  $-33^\circ$ .

## 2.3. Band 6 ALMA archival observations

We have complemented our 0.89 mm data with public ALMA archival data obtained in Band 6 (220.6 GHz, 1.3 mm) under projects 2016.1.00039.S (P.I. Dunham), and 2016.1.01284.S (P.I. Maury). We note that the former was observed with a comparable angular resolution as our 0.89 mm data. The description of these observations and the data reduction are included in Appendix A.

## 3. Main results

### 3.1. ALMA continuum data: most extended configurations

The 0.89 mm image of IRAM04191 is displayed in Figure 1 (left panel). The continuum emission is extended in the East-West direction, showing two bright sources separated by  $\sim 54$  mas ( $\sim 8$  au at 140 pc). The strongest emission is coming from the eastern-most source (IRAM04191E, hereafter). The two sources are surrounded by extended emission.

The 1.3 mm continuum data (project 2016.1.00039.S) is displayed in the middle panel of Fig. 1. It shows two emission peaks

separated by  $\sim 80$  mas (11 au at 140 pc). Similar to the 0.89 mm data, the brightest source is IRAM04191E, which is spatially resolved, while the western one (IRAM04191W) is point-like (see Table C.1). The 1.3 mm image also reveals extended emission connecting and surrounding the two sources.

The positions and fluxes for the two detected sources in the two bands are included in Table C.1. Note that, in the case of the 0.89 mm data, we have derived these parameters both in the self-calibrated (Fig. 1) and non self-calibrated images (see Appendix B for details).

The analysis of the ALMA data suggests that IRAM04191 could be part of a tight binary system. This is consistent with the fact that two ALMA sources separated by  $\sim 80$  mas are detected as compact sources in the two bands after applying a cut in  $uv$ -range of  $> 1100 k\lambda$  (see Figure B.2).

We have estimated the masses (gas plus dust) of the detected sources following the procedure described in Appendix D. Both show very low values between  $1.8$ - $0.4 M_{\text{Jup}}$  at 1.3 mm, and below  $1 M_{\text{Jup}}$  at 0.89 mm (see Table C.1). The mass of the whole emission (binary plus extended emission) is estimated to be  $4$ - $5 M_{\text{Jup}}$  at 0.89 mm, and  $4.1 M_{\text{Jup}}$  at 1.3 mm (see details in Appendix D).

### 3.2. VLA observations

The combined KKaQ-band image is displayed in the right panel of Figure 1. We have detected a single source at the position of IRAM04191 in the three observed bands (the three individual images are displayed in Figure E.1). The properties of this radio source are included in Table E.1. The image shows extended emission with an elongation towards the NE in the direction of the reported outflow (André et al. 1999). Using the fluxes at 33 and 22 GHz, we derive a spectral index of  $0.24\pm 0.23$ , consistent with free-free emission from a radio jet.

The bulk of the VLA emission seems associated to IRAM04191W, but the moderate angular resolution and sensitivity of the VLA data does not allow us to discern if the eastern component is also contributing to the centimeter emission. The position of the VLA source is offset by  $\sim 30$  mas south-east from IRAM04191W, which corresponds to the direction of the proper motion of Taurus members (e.g. Galli et al. 2019), although it is smaller than that reported for the neighboring moving groups (e.g. L1551, L1558), considering the time span of 7 years between the ALMA and VLA data. However, the different beam sizes and source morphologies in the ALMA and VLA data prevent a reliable determination of the proper motion. Dedicated observations are therefore required to characterize the nature of this positional offset and the proper motion of IRAM04191.

### 3.3. Molecular emission from $\text{C}^{18}\text{O}$ (2-1)

Maury (2020) has already suggested the presence of small disk around IRAM04191, so we have reanalyzed  $\text{C}^{18}\text{O}$  (2-1) observations to shed light on the system architecture. The moment 1 is displayed in Fig. 2, where we have selected the velocity channels that show emission close to the ALMA detections:  $3.5$ - $5.5$  km/s and  $7.9$  –  $9.4$  km/s. The velocity gradient in  $\text{C}^{18}\text{O}$  is consistent with material in rotation around the ALMA binary, confirming that it may be surrounded by a circumbinary disk whose geometrical center lies closer to the faintest source (IRAM04191W). The deconvolved size of the moment 0 of the  $\text{C}^{18}\text{O}$  (2-1) emission is  $0''.39\pm 0''.05 \times 0''.17\pm 0''.04$  (PA of  $88\pm 8^\circ$ ), which trans-

<sup>1</sup> [https://github.com/jjtobin/auto\\_selfcal](https://github.com/jjtobin/auto_selfcal)

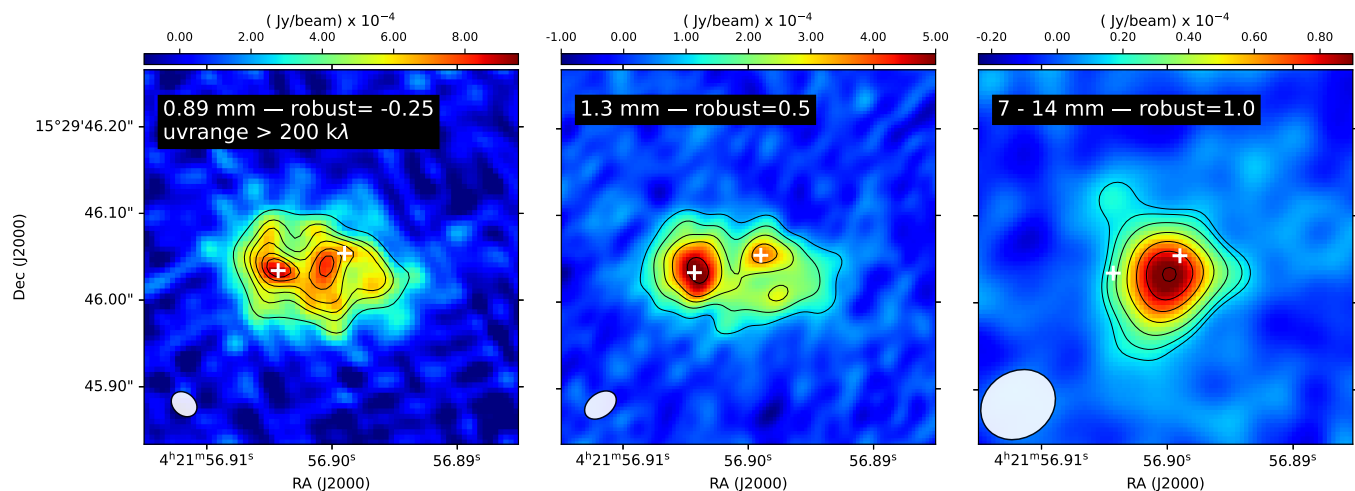


**Fig. 1.** ALMA and VLA observations of IRAM04191. Left: 0.89 mm observations. The contours represent values of 5, 7, 8, 9, 10, 10.7- $\sigma$  ( $rms=6.6e-05$  Jy/beam) drawn from the image smoothed with a Gaussian of FWHM corresponding to approximately one synthesized beam. Middle: 1.3 mm observations (robust of 0.5). The contours represent values of 4, 7, 10, 13, and 19- $\sigma$ , with  $rms=2.4e-05$  Jy/beam. Right: VLA KKaQ image (robust of 1). The contours correspond to 3, 4, 6, 9, 12, 15, 18 times the  $rms$  ( $5 \mu Jy/beam$ ). The synthesized beams are displayed in the bottom left corner of each image. The white crosses represent the positions of the two detected sources at 1.3 mm.

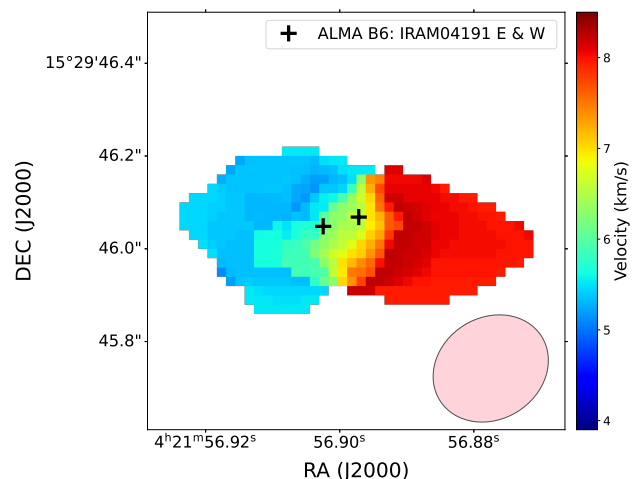


**Fig. 2.** First-order moment of the  $C^{18}O(2-1)$  line. We have selected the channels that show emission closer to the central binary (see text), revealing the presence of rotating emission resembling a circumbinary disk. The synthesized beam is displayed at the bottom right (pink). We have overplotted with black contours the detection from the ALMA 1.3 mm observations, being 4, 7, 10, 13, 19 the  $rms$  of the image,  $2.4e-5$  Jy/beam. The beam of the ALMA data is shown in the bottom-left corner (grey). The red and black '+' signs indicate the positions of the sources detected at 1.3 mm, as reported in Table B1.

lates into a disk radius of  $\sim 27$  au, and an inclination<sup>2</sup> of  $64 \pm 7^\circ$ , in good agreement with the values of  $50-60^\circ$  derived in previous works (e.g. André et al. 1999).

We have used the moment 1 of the  $C^{18}O$  emission to generate a  $pv$  diagram along its major axis which, as shown in Fig. 3 shows a Keplerian-like pattern. We have fitted the  $pv$ -diagram using the SLAM code (Sai 2023), and adopting both the edge and ridge methods. We assumed a  $rms$  noise of 2.45 mJy, an SNR threshold of 5, and Gaussian weighting. The ridge method

<sup>2</sup> Estimated using the size ratio between major and minor disk axes following the expression  $\cos^{-1}(\theta_{min}/\theta_{maj})$

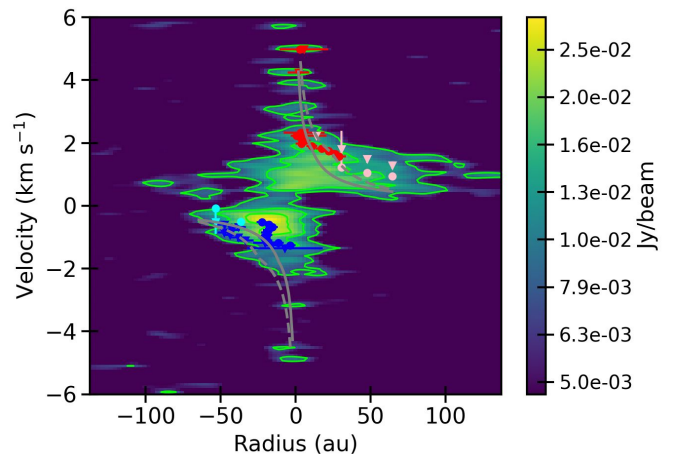


**Fig. 3.**  $PV$ -diagram built along the major axis of the  $C^{18}O$  emission. The contours represent values of 3, 6 and 9- $\sigma$ . We include the extracted velocities from the edge (pink and cyan) and ridge (blue and red) methods within SLAM, assuming a Keplerian rotation pattern.

provides a more robust tracing of the emission, yielding a break radius of  $\sim 11$  au and a dynamical mass of  $0.05 \pm 0.04 M_\odot$ .

#### 4. Discussion

The ALMA data presented here has allowed us for the first time to (i) resolve IRAM04191 into a tight Class 0 substellar binary candidate with  $\sim 11$  au of projected separation surrounded by a circumbinary disk centered on the faintest ALMA continuum source (IRAM04191W), and (ii) estimate a dynamical of  $\sim 50 \pm 40 M_{Jup}$  for the whole system. In the context of Class 0 binary systems, IRAM04191 would represent one of the tightest binaries detected in continuum emission to date, only comparable to L1157 MMS, a 16 au Class 0 binary (Tobin et al. 2022).

A two-peak morphology in the continuum emission of a young object can be also interpreted as a high-inclined disk with a large inner cavity. However, such a large cavity would be hard to reconcile with the strong molecular outflow reported in this

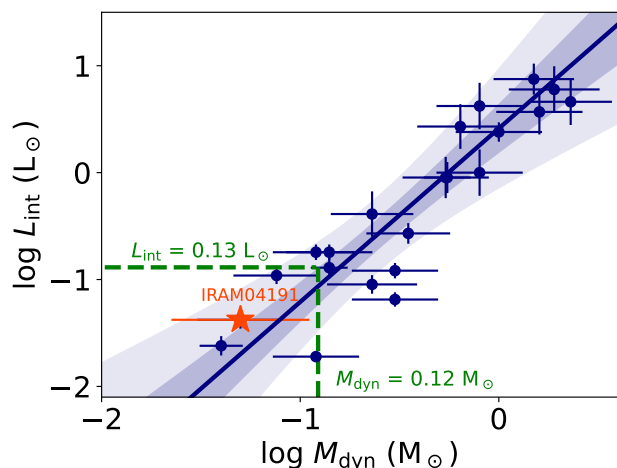


**Fig. 4.** Dynamical mass ( $M_{\text{dyn}}$ ) vs  $L_{\text{int}}$  diagram adopted from Palau et al. (2024). Blue symbols represent protostars, VeLLOs and proto-BD candidates with  $L_{\text{int}}$  and  $M_{\text{dyn}}$  measurements, while the solid line represents the fit to the data. The shaded area corresponds to 2 (dark) and 5 times (light) the uncertainty of the fit. The dashed green lines delimit the region at the bottom left consistent with proto-BDs. We have represented IRAM 04191 with the dynamical mass derived in this work.

source, and the presence of a radio jet normally associated with very young objects. Moreover, in an edge-on disk scenario, the VLA centimeter detection presented here would be expected to lie between the two ALMA peaks, which is not the case.

Considering that IRAM04191W seems associated to the VLA detection and its location at the center of the circumbinary disk, it is reasonable to suggest that this source may be the primary (and hence, most massive) component of the binary, despite being the fainter emitter in the ALMA data. A comparable configuration was observed in the protostellar binary [BHB2007] 11 (Alves et al. 2019), although in this case both components were detected in the VLA data. In any case, this hypothesis needs further confirmation through future dedicated ALMA and VLA observations.

Palau et al. (2024) presented a correlation between the dynamical mass ( $M_{\text{dyn}}$ ) of protostars and VeLLOs with their  $L_{\text{int}}$ . We have represented IRAM04191 in this diagram taking advantage of the mass derived in this work, and it is found to be consistent with the established correlation, strongly suggesting its substellar nature (Fig. 4). Since the object is a binary, the individual values for both parameters should be divided taking into account the binary mass ratio, which is currently unknown.

The reported values of  $M_{\text{env}}$  for IRAM04191 vary between  $0.05 M_{\odot}$ , using Herschel/SPIRE data at  $250 \mu\text{m}$  (Kim et al. 2016), and  $0.5 M_{\odot}$  using  $1.3 \text{ mm}$  data (André et al. 1999). The discrepancy between values is mainly related with the different methodology to estimate the mass, using different radius ( $24''$  vs  $60''$ , respectively) to integrate the flux. We have reanalyzed the SPIRE/ $250 \mu\text{m}$  data of IRAM04191 and estimated a  $M_{\text{env}}$  of  $\sim 0.2 M_{\odot}$  integrating the flux within a  $4\text{-}\sigma$  contour around the source, and assuming  $T_{\text{dust}}$  and opacity as in Kim et al. (2016). Adopting a star formation efficiency of 30% (see e.g. Palau et al. 2024), we can infer a mass reservoir of  $\sim 60 M_{\text{Jup}}$  available to be accreted by the binary over its evolution. Assuming a very conservative mass of  $45 M_{\text{Jup}}$  for each of the binary components, and that each accretes half of the mass reservoir, the system might end up as a substellar pair. We note, however, that different works have reported episodic accretion onto the source (Lee 2007; Anderl et al. 2020). This, combined with the occurrence

of mass-loss episodes (e.g. molecular outflow, radio jet), implies that the fate of the binary cannot be definitely established.

Early in the formation process, turbulent fragmentation produces binaries with initial separations wider ( $>500 \text{ au}$ ) than those formed by disk fragmentation, although dynamical evolution can quickly change these separations to lower values in  $\sim 0.1 \text{ Myr}$  (Offner et al. 2016). In that respect, core fragmentation models by Bate (2009, 2012) can produce very low-mass binaries with small separations ( $<40 \text{ au}$ ), although the cloud properties do not resemble those of Taurus. An observational test to shed light on the formation mechanism of IRAM04191, would be to study the misalignment of the outflows and/or disks of the two components with future more sensitive ALMA observations (Offner et al. 2016). Interestingly, most BD binaries observed in the field and star forming regions are tight systems (sep  $<10\text{-}20 \text{ au}$ ) with mass ratio close to 1 (e.g. Duchêne & Kraus 2013). The confirmation of IRAM04191 as a compact binary candidate at such early evolutionary stage would raise the question whether the separation distribution observed in more evolved systems could be set at very early stages of BD binary formation.

*Acknowledgements.* We are indebted to an anonymous referee that has improved the paper with a very constructive report. This research is funded by the Spanish grant MCIN/AEI/10.13039/501100011033 PID2023-150468NB-I00. NH is grateful to ESO-Chile for hosting her through the Visitor’s Program 2024, and the IRyA for hosting her through project UNAM-PAPIIT IG100223. A.P. acknowledges financial support from the UNAM-PAPIIT IN120226 grant, and the Sistema Nacional de Investigadores of SECIHTI, México. CC-G acknowledges support from UNAM DGAPA PAPIIT grant IG101224 and from CONAHCyT Ciencia de Frontera project ID 86372. This work benefited from the UNAM-NRAO Memorandum of Understanding in the framework of the Next Generation Very Large Array (ngVLA) Project (MOU-UNAM-NRAO-2023). N. Otten acknowledges funding from the Maynooth University Graduate Teaching Scholarship and Taighde Éireann (Research Ireland) under the RI-ESO Studentship Agreement for this work. This paper makes use of the following ALMA data: ADS/JAO.ALMA#2017.1.00551.S, 2016.1.00039.S, and 2016.1.01284.S. ALMA is a partnership of ESO (representing its member states), NSF (USA) and NINS (Japan), together with NRC (Canada), MOST and ASIAA (Taiwan), and KASI (Republic of Korea), in cooperation with the Republic of Chile. The Joint ALMA Observatory is operated by ESO, AUI/NRAO and NAOJ. The National Radio Astronomy Observatory and Green Bank Observatory are facilities of the U.S. National Science Foundation operated under cooperative agreement by Associated Universities, Inc.

## References

- Alves, F. O., Caselli, P., Girart, J. M., et al. 2019, *Science*, 366, 90  
 Anderl, S., Maret, S., Cabrit, S., et al. 2020, *A&A*, 643, A123  
 André, P., Motte, F., & Bacmann, A. 1999, *ApJ*, 513, L57  
 Bate, M. R. 2009, *MNRAS*, 392, 590  
 Bate, M. R. 2012, *MNRAS*, 419, 3115  
 di Francesco, J., Evans, II, N. J., Caselli, P., et al. 2007, *Protostars and Planets V*, 17  
 Duchêne, G. & Kraus, A. 2013, *ARA&A*, 51, 269  
 Dunham, M. M., Evans, II, N. J., Bourke, T. L., et al. 2006, *ApJ*, 651, 945  
 Galli, P. A. B., Loinard, L., Bouy, H., et al. 2019, *A&A*, 630, A137  
 Kim, M.-R., Lee, C. W., Dunham, M. M., et al. 2016, *ApJS*, 225, 26  
 Lee, J.-E. 2007, *Journal of Korean Astronomical Society*, 40, 83  
 Maury, A. 2020, in *IAU Symposium*, Vol. 345, *Origins: From the Protosun to the First Steps of Life*, ed. B. G. Elmegreen, L. V. Tóth, & M. Güdel, 91–95  
 McMullin, J. P., Waters, B., Schiebel, D., Young, W., & Golap, K. 2007, in *Astronomical Society of the Pacific Conference Series*, Vol. 376, *Astronomical Data Analysis Software and Systems XVI*, ed. R. A. Shaw, F. Hill, & D. J. Bell, 127  
 Offner, S. S. R., Dunham, M. M., Lee, K. I., Arce, H. G., & Fielding, D. B. 2016, *ApJ*, 827, L11  
 Ossenkopf, V. & Henning, T. 1994, *A&A*, 291, 943  
 Palau, A., Huélamo, N., Barrado, D., Dunham, M. M., & Lee, C. W. 2024, *New A Rev.*, 99, 101711  
 Sai, J. 2023, SLAM: A PV-diagram fitting tool for disk kinematics, <https://github.com/jinshisai/SLAM>, gitHub repository  
 Tobin, J. J., Cox, E. G., & Looney, L. W. 2022, *ApJ*, 928, 61  
 Tobin, J. J., Sheehan, P., Xue, R., & Fourkas, A. 2025, *jitobin/auto\_selfcal*: v2.0.0

## Appendix A: ALMA archival data reduction

The 1.3 mm data from project 2016.1.00039.S (P.I. Dunham) were obtained on November 1st 2017, only  $\sim 3$  weeks before our 0.89 mm observations. The data were obtained with 49 antennas of the 12-array in single field dual-polarization mode, dedicating one spectral window of 1.875 GHz bandwidth to observe continuum and five more spectral windows to observe spectra line emission, comprising an aggregate bandwidth of 2.262 GHz. The average precipitable water-vapor column of the observations was  $\sim 0.5$  mm. The baselines ranged from 113 m to 13.9 km. The maximum recoverable scale was  $0''.5$ . Bandpass and flux calibrations were made using QSO J0510+1800, while QSO J0431+1731 was used as a phase calibrator. The science time on-source was 31 minutes. Data were calibrated using the CASA pipeline, version 5.1.1. Continuum imaging was performed using the task `tclean` in multi-frequency synthesis mode and a multi-scale clean deconvolution algorithm with scales of 0,  $0''.04$ , and  $0''.1$ . A cellsize of  $0''.004$  was used, with Briggs weighting and a robust parameter = 0.5, providing a synthesized beam of  $0''.04 \times 0''.03$  and PA of  $-36^\circ$ . We tried the self-calibration of the data, but it did not work due to the faintness of the source. The uvrage of the data spans from 53 to  $9200 k\lambda$ .

We have also analyzed data from project 2016.1.01284.S (P.I. Maury), which were obtained in two executions on October 15, 2016, and July 21, 2017. Observations were taken with 41 and 46 antennas of the 12-array respectively, in single field dual-polarization mode. Three spectral windows of 1.875 GHz bandwidth each were set up to observe continuum, and four more spectral windows of 58.594 MHz bandwidth were selected to observe spectra line emission, comprising an aggregate bandwidth of 5.859 GHz. The average precipitable water-vapor column of the observations was  $\sim 0.64$  mm. The baselines ranged from 16.7 m to 3.7 km. The maximum recoverable scale was  $1''.9$ . Bandpass calibration was made using QSO J0425+1755 and J0237+2848. QSO J0425+1755 and J0423-0120 were used for flux calibration, and QSO J0433+0521 and J0449+1121 were used as phase calibrators respectively. The total time on the science source was 1.1 hr. Data were calibrated using version 4.7.2 of the CASA pipeline. For this paper, we have only analyzed the spectral window that covered the emission at  $C^{18}O$  (2-1), with 61.035 kHz spectral resolution, equivalent to 0.08 km/s velocity resolution. We note that this dataset was already discussed in Maury (2020), who already suggested the presence of a small disk around the source. We have reprocessed the data to isolate the disk emission in order to (i) study its location with respect to the binary components, and (ii) to estimate a dynamical mass for the whole system.  $C^{18}O$ (2-1) imaging was performed using the task `tclean` using `hogbom` cleaning deconvolution algorithm. A cell size of  $0''.02$  was used, with Briggs weighting and a robust parameter = 1.5, providing a synthesized beam of  $0''.3 \times 0''.2$ , and PA of  $-57.8^\circ$ . CASA version 6.5.6 was used for imaging purposes.

## Appendix B: ALMA Band 7 data

To further investigate the presence of two compact sources in the ALMA data, we have compared different data reductions with different robust parameters and a cut in uvrage  $> 200 k\lambda$ . We have explored robust of 0.5, 0.3, -0.25, -0.5 and -1, and we display the images with -0.25 and 0.5 in Figs. 1 and B.1, respectively. The left panel of Fig. B.1 shows the 0.89 mm image with robust 0.5, in which we detect a central source resolved into two bright peaks separated by  $0''.04$ , and an additional extended emis-

sion towards the north-west, in the direction where we detect the secondary component in the 1.3 mm data. As the robust is decreased, giving more weight to the longest baselines, the two central peaks set apart, and show a separation of  $\sim 0''.054$  for a robust of -0.25, as shown in Section 2.1). Although this particular robust allows us to resolve the binary, it has the disadvantage of increasing the image noise ( $rms$   $6.6e-5$  Jy/beam) in comparison with the robust of 0.5 ( $4.9e-5$  Jy/beam).

For comparison, the panel on the right of Fig. B.1 shows the non-self-calibrated 0.89 mm image obtained using a robust of 0.5. For this data, the calibration was done with CASA version 5.1.1. To produce the continuum image shown in the figure, we used a more recent version of CASA (6.5.6). The task `tclean` was used in multifrequency synthesis mode, with multiscale clean deconvolution algorithm comprising scales of 0,  $0''.02$ , and  $0''.1$ . We used a cellsize of  $0''.004$ , with Briggs weighting and robust parameter of 0.5, providing the best trade-off between spatial resolution and sensitivity. The resulting synthesized beam is  $0''.05 \times 0''.03$ , and position angle of  $40.4^\circ$ . This image allows us to recover the two components of the binary system more easily because the extended emission is decorrelated and artificially spread along the northeast-southwest direction, revealing more clearly the central emission. The resulting image shows an  $rms$  of  $4.5e-5$  Jy/beam, better than the value obtained in the self-calibrated image with robust -0.25. Hence, we have also used this image to derive the physical parameters of the binary components included in Table C.1.

Due to the fact that a negative robust enhances artificial clumpy emission, we have also generated a 0.89 mm self-calibrated image with robust of 0.5 and a cut in uvrage of  $uvrange > 1100 k\lambda$ , giving more weight to the most extended baselines. The result is displayed in Fig. B.2 (left panel). The image with the uv cut shows a strong source to the east plus an additional well-separated source to the west at a separation of  $\sim 80$  mas. The two bright emissions are connected by a stream of material. For comparison, we have also applied a cut in uvrage of  $> 1100 k\lambda$  to the 1.3 mm image (B.2, right panel), recovering the reported binary with the detection of two compact sources at a separation of  $\sim 80$  mas.

## Appendix C: ALMA parameters of the sources detected at 0.89 mm and 1.3 mm continuum images.

Table C.1 includes the coordinates, peak intensities, fluxes, and deconvolved sizes of the two sources detected in the 0.89 mm and 1.3 mm ALMA images. Note that, for the reasons explained above, the 0.89 mm measurements have been performed both in the self-calibrated image shown in Figure 1, and in the non self-calibrated image displayed in the right panel of Figure B.1. The ALMA flux calibration accuracy is  $\sim 10\%$  in the two bands (see e.g. 10.5281/zenodo.4511522). Positions and peak intensities of the two sources have been derived using `imstat`. A double Gaussian has been fitted to the most compact emission of the data to estimate the flux density and the deconvolved size of the two binary components in the two bands.

## Appendix D: Estimation of masses from ALMA continuum data

We have estimated the mass of the ALMA sources assuming optically thin and isothermal dust emission, and following the expression:

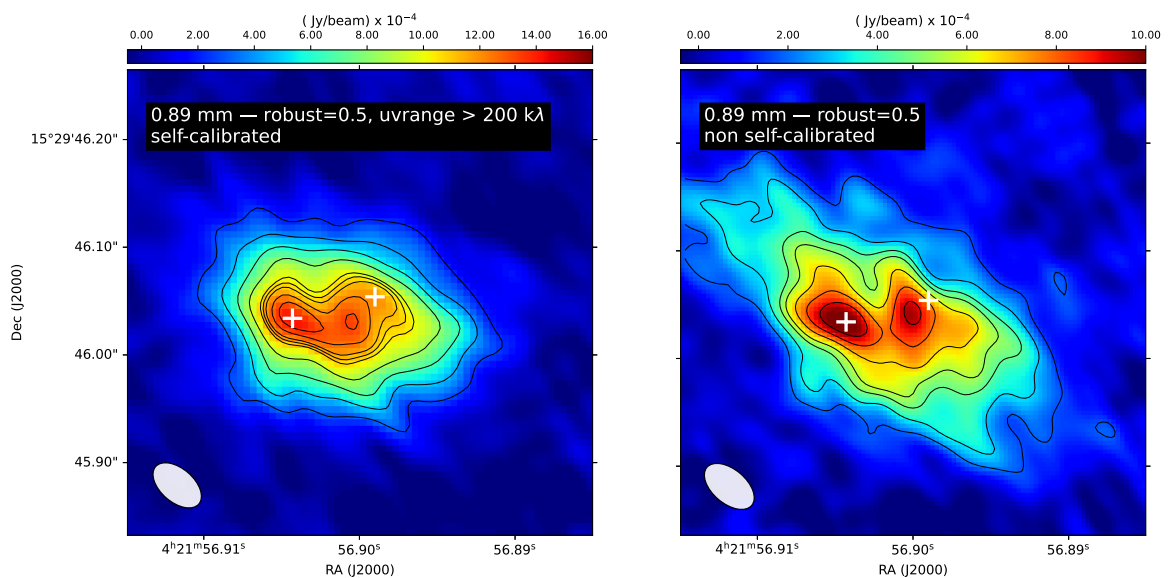


**Fig. B.1.** 0.89 mm observations of IRAM04191 with robust of 0.5. Left: self-calibrated image. The contours represent 5, 9, 13, 17, 21, 22, 23, 25, 27 times the  $rms$  ( $4.9e-5$  Jy/beam). Right: non self-calibrated image. The contours represent 4, 7, 10, 12, 15, 18, 21 times the  $rms$  ( $4.5e-5$  Jy/beam). The white crosses represent the position of the two sources detected in the 1.3 mm data.

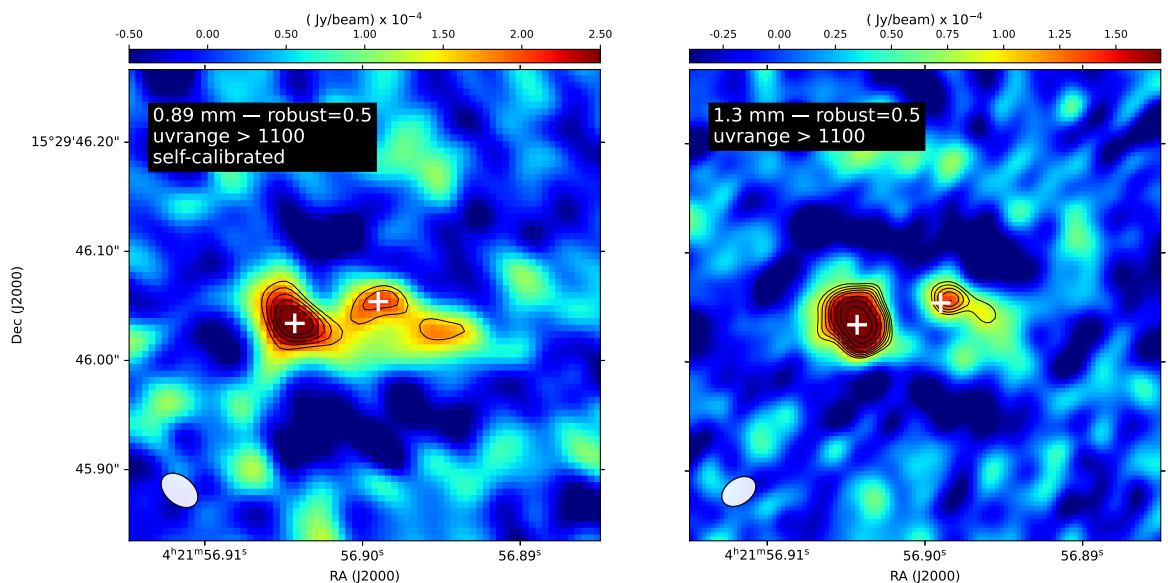


**Fig. B.2.** Observations of IRAM04191 with  $uvrange > 1100$  k $\lambda$ . The images are smoothed with a Gaussian of FWHM approximately equal to the synthesized beam. The contours in the two images represent 3, 3.5, 4, 4.5, 5, 6, 7, 8 times the  $rms$ . Left panel: 0.89 mm data ( $rms = 5.4e-5$  Jy/beam); Right panel: 1.3 mm data ( $rms = 2.8e-5$  Jy/beam). The white crosses represent the position of the two sources detected in the 1.3 mm data with full range displayed in Fig. 1.

$$M_{\text{dust}} = \frac{F_{\nu} d^2}{k_{\nu} B_{\nu}(T_d)}, \quad (\text{D.1})$$

where  $F_{\nu}$  is the flux density at the given frequency,  $d$  is the distance to the source,  $k_{\nu}$  is the dust mass opacity, and  $B_{\nu}(T_d)$  is the Planck function at the dust temperature  $T_d$ . We have assumed a dust temperature of 12.5 K (André et al. 1999), opacities of 1.68 and 0.89  $\text{cm}^2/\text{g}$  for 890  $\mu\text{m}$  and 1.3 mm (for thin ice mantles and density of  $10^{-6}$   $\text{cm}^3$ ), respectively (Ossenkopf & Henning 1994), and a gas-to-dust mass ratio of 100. The masses are included in the last column of Table C.1. We have also estimated the mass of the whole integrated emission (binary plus

extended emission) in both bands. To do so, we have first integrated the whole emission within a  $3\sigma$  contour in the images, resulting in density fluxes of  $14.3 \pm 0.4$  (self-calibrated, Fig. 1) and  $17.4 \pm 0.2$  mJy (non self-calibrated, right panel of Fig. B.1) in the 0.89 mm images, and  $4.4 \pm 0.1$  mJy at 1.3 mm. Using equation D, we derive masses of  $\sim 4 M_{\text{Jup}}$  and  $\sim 5 M_{\text{Jup}}$  for the self- and non-self-calibrated images at 0.89 mm, and  $\sim 4 M_{\text{Jup}}$  at 1.3 mm.

## Appendix E: VLA observations of IRAM04191

We have detected a single source in the VLA observations presented in Section 3.2. Figure E.1 shows the individual images in the K, Ka, and Q bands, while Table E.1 summarizes the proper-

**Table C.1.** Properties of the ALMA detected emissions towards IRAM04191

Source	RA(J2000) (hh:mm:ss)	DEC(J2000) (dd:mm:ss)	Peak <sup>1</sup> Intensity (mJy/beam)	Flux <sup>2</sup> Density (mJy)	Deconvolved <sup>3</sup> size (mas, °)	Mass (M <sub>Jup</sub> )
Band 7 (2017.1.00551.S) – self-calibrated image						
IRAM04191E	04:21:56.9044	15:29:46.035	0.91±0.07	1.63±0.19	37.8±0.2×15.7±0.4, PA=49±7	0.45
IRAM04191W	04:21:56.9007	15:29:46.041	0.81±0.07	1.16±0.15	point-like	0.32
Band 7 (2017.1.00551.S) – non self-calibrated image						
IRAM04191E	04:21:56.9046	15:29:46.034	1.07±0.04	1.98±0.10	58.43±0.08 × 24.5±0.2, PA=43±3	0.54
IRAM04191W	04:21:56.9001	15:29:46.042	0.97±0.04	1.28±0.08	37.4±0.8 × 8.2±6.0, PA=14±5	0.35
Band 6 (2016.1.00039.S)						
IRAM04191E	04:21:56.9043	15:29:46.034	0.52±0.02	1.89±0.06	64.5±0.2 × 41.4±0.3, PA=54±10	1.75
IRAM04191W	04:21:56.8990	15:29:46.054	0.38±0.02	0.48±0.04	point-like	0.45

Notes to table: <sup>1</sup> The reported error is the *rms* of the map; <sup>2</sup> Flux density inferred from a double Gaussian fitting to the most compact emission of the data; <sup>3</sup> Estimated from a double Gaussian fitting to the data. We provide the size and the PA.

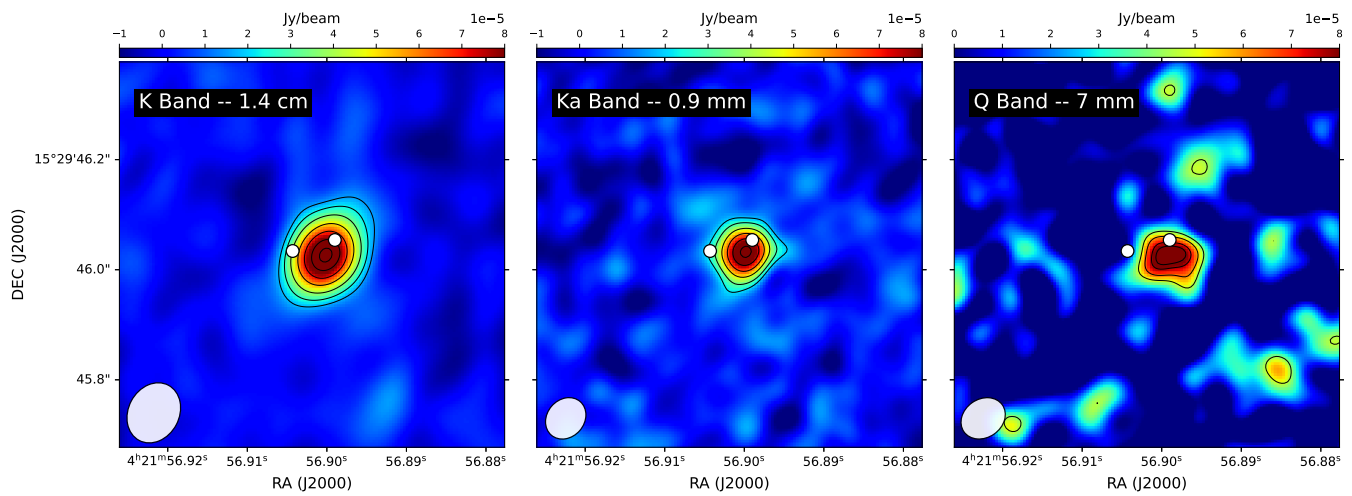


**Fig. E.1.** VLA images of IRAM04191 in the three observed bands: 1.4 cm (left), 9 mm (middle) and 7 mm (right). The first panel shows contours at 4, 6, 9, 13, 17, 21, 24 × the *rms* (4 μJy/beam) and the second panel 4, 6, 9, 12, 15, 18 × *rms* (5 μJy/beam). The 7 mm image displays contours representing 3, 4, 5, and 5.5 × *rms* (15 μJy/beam). Natural weighting is used in all three images; the 7 mm image includes a 2000 *kλ* taper.

**Table E.1.** Properties of the VLA detected source

Band	$\nu$ (GHz)	$\lambda$ (cm)	RA(J2000) (hh:mm:ss)	DEC(J2000) (dd:mm:ss)	Peak Intensity (μJy/beam)	Flux Density (μJy)	Deconvolved Size <sup>1</sup> (mas, °)	Beam Size <sup>1</sup> (mas, °)
K	22	1.40	04:21:56.900	15:29:46.026	98±3	118±6	60×40±10, PA=144±30	113×92, PA=-27.9
Ka	33	0.90	04:21:56.900	15:29:46.030	93±5	130±10	44×42±20, PA=144±30	80×68, PA=-40.7
Q	44	0.68	04:21:56.900	15:29:46.020	93±7	180±20	90×50±20, PA=70±20	85×70, PA=-55.0

Notes: for K and Ka, the measurements are obtained on the images with natural weighting, while for Q they are measured on the images with natural weighting and a taper of 2000 *kλ*; <sup>1</sup> We provide the size in *mas* and the position angle (PA) in degrees, with their associated uncertainties; <sup>2</sup> We provide the beam size and its position angle (PA).

ties of the detected source in the three bands. Note that the flux calibration uncertainties in K, Ka and Q-bands are of 10-12%<sup>3</sup>.

<sup>3</sup> <https://science.nrao.edu/facilities/vla/docs/manuals/oss/performance/fdscale>